Geomorphology 426 (2023) 108590

Contents lists available at ScienceDirect

Geomorphology

journal homepage: www.journals.elsevier.com/geomorphology

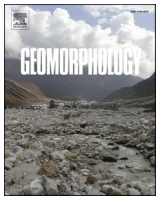

Gradual versus episodic lateral saltmarsh cliff erosion: Evidence from Terrestrial Laser Scans (TLS) and Surface Elevation Dynamics (SED) sensors

Daphne van der Wal [a,b,*], Jeroen van Dalen [a], Pim W.J.M. Willemsen [a,c,d], Bas W. Borsje [c], Tjeerd J. Bouma [a]

[a] NIOZ Royal Netherlands Institute for Sea Research, Dept Estuarine and Delta Systems, P.O. Box 140, 4400 AC Yerseke, the Netherlands
[b] Faculty of Geo-Information Science and Earth Observation (ITC), University of Twente, P.O. Box 217, 7500 AE Enschede, the Netherlands
[c] Faculty of Engineering Technology, Department of Water Engineering & Management, University of Twente, P.O. Box 217, 7500 AE Enschede, the Netherlands
[d] Deltares, Department of Ecosystems and Sediment Dynamics, P.O. Box 177, 2600 MH Delft, the Netherlands

ARTICLE INFO

Keywords:
Saltmarsh
Mudflat
Erosion
Wave energy

ABSTRACT

As lateral erosion can threaten valuable saltmarsh habitats and their capacity to protect the hinterland from waves and floods, there is a need to understand the mechanisms of erosion. We monitored lateral saltmarsh erosion at high spatiotemporal resolution during a 2.5 year period. We performed terrestrial laser scans (TLS) with centimetric spatial resolution, ca monthly, as well as before and after 2 wind events to assess morphological change of a saltmarsh cliff (<0.8 m in height), and deployed surface elevation dynamics (SED) sensors at 3 locations to obtain daily measurements of the cliff edge position with 2 mm resolution. This was complemented by wind data, and a pressure transducer on the mudflat to obtain time-series of local inundation duration, water depth, wave height, period, power and energy. TLS shows gradual lateral erosion of the marsh edge and surface, and occasional local slumping, with substantial local variation. SED sensor data also reveal that lateral erosion was mostly continuous, with episodes with stronger and weaker local erosion, at all 3 locations, often correlated in space. Correlations between changes in total marsh area and sediment volume of the mudflat-saltmarsh interface from TLS with particularly inundation duration and wind velocity were discussed. At plot level, correlations were not consistent; correlations between the local lateral erosion rates and hydrodynamics/winds were not significant. Results emphasize the importance of common low magnitude events for long-term lateral erosion.

1. Introduction

Saltmarshes are ecosystems inhabited by salt-tolerant plants that are inundated by tides and waves. They provide valuable ecosystem services, for example as a habitat for a range of aquatic and terrestrial species and as a buffer to reduce the risk of flooding of the hinterland by attenuating hydrodynamic energy (Costanza et al., 1997; Bouma et al., 2014; Möller et al., 2014). Regular flooding allows trapping of sediment in the vegetation (Knutson et al., 1982; Stumpf, 1983; Ma et al., 2018). This enables saltmarshes to keep up with sea level rise, when sufficient supply of sediment is available (Fagherazzi et al., 2012; Kirwan and Megonigal, 2013; Best et al., 2018).

Apart from vertical sediment dynamics, saltmarshes are subject to lateral sediment dynamics. They can expand laterally through seedling establishment or rhizome growth given suitable conditions (e.g., McKee and Patrick, 1988; Feist and Simenstad, 2000; Hammond et al., 2002; van der Wal et al., 2002; Dennis et al., 2011; Hu et al., 2015a, 2015b). The saltmarsh edge can also retreat laterally through cliff erosion, of the order of centimetres to metres per year (e.g., van der Wal et al., 2008; Fagherazzi et al., 2013). Sediment from lateral retreat may promote vertical accretion of the saltmarsh, as shown by Mariotti and Carr (2014).

Periods of lateral expansion of the saltmarsh vegetation and retreat of saltmarsh area due to cliff erosion may alternate. Pringle (1995) identified alternating periods of saltmarsh erosion and expansion at a scale of years to decades and attributed these to shifts in position of the channel fronting the saltmarsh-mudflat system. In a review on autocyclicity of saltmarshes, Singh Chauhan (2009) pointed to the mutual interactions of the saltmarsh and mudflat, where changes of the tidal flat relative to the water level either promote or restrict marsh growth. Van

* Corresponding author at: NIOZ Royal Netherlands Institute for Sea Research, Dept Estuarine and Delta Systems, P.O. Box 140, 4400 AC Yerseke, the Netherlands.
E-mail address: Daphne.van.der.Wal@nioz.nl (D. van der Wal).

https://doi.org/10.1016/j.geomorph.2023.108590
Received 10 May 2022; Received in revised form 31 December 2022; Accepted 12 January 2023
Available online 16 January 2023

de Koppel et al. (2005) have explained such saltmarsh cycles by self-organisation. Feedbacks between plant growth, flow attenuation and sedimentation may result in steepening of the marsh edge with an increased vulnerability of the marsh face to disturbances, such as storms, which may then result in continued erosion of the marsh cliff (Van de Koppel et al., 2005). When extrinsic conditions are not limiting, pioneer saltmarsh can then re-establish on the higher mudflat, just seaward of the saltmarsh edge, trapping sediment and forming a buffer against erosion (Van de Koppel et al., 2005; van der Wal et al., 2008; Wang et al., 2017). Likewise, slumped material can be deposited just in front of the cliff and prevent further lateral erosion (Gabet, 1998).

The drivers of lateral saltmarsh erosion rates remain still poorly understood. Lateral retreat of the saltmarsh is attributed to overall limited sediment supply in the mud-saltmarsh system (van der Wal et al., 2008; Fagherazzi et al., 2013; Ladd et al., 2019; Schuerch et al., 2019). Such conditions may hinder expansion and re-establishment of vegetation or facilitate cliff erosion (e.g., Van de Koppel et al., 2005; Tommasini et al., 2019). Local sediment dynamics may also play a key role in the process of cliff-formation, and seedling re-establishment in front of a cliff may be hindered when bed level variability is high (Bouma et al., 2016; Cao et al., 2018; Willemsen et al., 2018; Willemsen et al., 2022).

Wave forcing is recognized as a key variable in explaining lateral saltmarsh erosion (e.g., Schwimmer, 2001; Huff et al., 2019), regulating local sediment dynamics and redistribution of sediments (Bouma et al., 2016; Willemsen et al., 2018; Leonardi et al., 2018). Local wave conditions depend on bathymetry and water level (determining water depth), wind energy and fetch. Several studies have shown how the bathymetry of the foreshore fronting the marsh is important for attenuating waves before they reach the cliff edge (Cooper, 2005; Callaghan et al., 2010; Hu et al., 2015b). For a given marsh, waves at the mudflat can hence be taken as indicative of what happens near the cliff edge (e.g., Willemsen et al., 2020). Mariotti and Fagherazzi (2013) also show the influence of bathymetry on bottom shear stresses, which in turn affect bathymetry and sediment availability. Morphological changes on the mudflat, such as lowering of the tidal flat, may induce changes in the local wave power, resulting in changes in the rate of erosion of the marsh edge (Tommasini et al., 2019). Such changes in environmental conditions, either natural or by human impacts, have also been related to lateral erosion in other studies (van der Wal and Pye, 2004; Marani et al., 2011; Siemes et al., 2020).

Marani et al. (2011) proposed a linear relationship between the mean annual wave power and the rate of volumetric marsh edge retreat. Leonardi et al. (2016a) demonstrated this linear relation between wave power and erosion rate using a global data set, suggesting that extreme events (storms) do not contribute hugely to the erosion rate. This aligns with the frequency-magnitude theory by Wolman and Miller (1960), who found that the bulk of the sediment is transported, by rivers or wind, under moderate events, rather than rare extreme events. Leonardi et al. (2016a) state that in the US, violent storms and hurricanes contribute <1 % to long-term salt marsh erosion rates, whereas the highest contribution comes from moderate but frequent weather conditions. They noted that saltmarsh erosion occurs even under low wave energy conditions.

The rate of lateral saltmarsh retreat may also be modulated by the erodibility of the saltmarsh. This erodibility of the saltmarsh, particularly its resistance to waves, may depend on, for example the sediment properties (such as grain-size distribution of the sediment, bulk density, cohesion, presence of cracks and fissures) of the marsh cliff edge, and vegetation traits and state (e.g., root density, above-ground biomass, expansion mode and rate), and their interaction (cf. Allen, 1989; Feagin et al., 2009; Wang et al., 2017; Lo et al., 2017; Bendoni et al., 2019; Marin-Diaz et al., 2021).

Leonardi et al. (2016a) observed that salt marshes did not collapse with increasing wave energy, highlighting the intrinsic endurance of salt marshes against extreme events. However, Francalanci et al. (2013) and Bendoni et al. (2014, 2016) suggest a non-linear relation between wave exposure and lateral erosion rates. They indicate the presence of a vertical gradient in erodibility along the marsh scarp (i.e., compaction at the saltmarsh surface by vegetation, and impact of wave breaking at the marsh base), promoting cantilever failures and erosion. Young and Ashford (2008) describe a similar process of undercutting of the marsh edge by waves, creating catastrophic cliff failures. Mass failure may be expected to generate a non-linear response in the wave power – erosion rate relationship. Recently, Mel et al. (2022) conducted a local study at different temporal scales using erosion pins placed in the saltmarsh cliff edge, revealing a linear relationship between the wave power and the erosion rate, with the regression slope depending on elevation (i.e., position on the vertical profile) and on the occurrence of mass collapse; months with higher waves typically had more frequent mass movement.

In order to quantify the lateral erosion rates of saltmarshes, appropriate techniques are required. The lateral dynamics of saltmarshes have been quantified using in situ and remote sensing techniques. *Firstly*, erosion pins placed in the cliff edge have been traditionally used to quantify the rate of lateral erosion (e.g., Gabet, 1998; Mel et al., 2022). *Secondly*, conventional ground surveying equipment (theodolite, Total Station (EDS) or dGPS) have been used to assess lateral changes in the saltmarsh edge, e.g. of cross-shore transects (e.g., van der Wal and Pye, 2004; van der Wal et al., 2008). *Thirdly*, airborne laser altimetry (Cracknell, 1999; Saye et al., 2005) tripod-based Terrestrial Laser Scanners (TLS) (Shilpakar et al., 2016; Huff et al., 2019), and in situ handheld mobile Terrestrial Laser Scanners (TLS) (James and Quinton, 2014) provide synoptic, detailed elevation measurements. TLS has been used to monitor sea cliffs (Young and Ashford, 2008; Young et al., 2010) and recently also lateral erosion of saltmarsh cliffs (Huff et al., 2019). Sequential remote sensing imaging techniques also allow synoptic assessment of morphological changes, such as aerial photography or UAV (drones) (Smith and Zarillo, 1990; van der Wal et al., 2008; Hu et al., 2015b), while near-surface remote sensing with cameras coupled to photogrammetric or Structure from Motion techniques (e.g., Nieuwhof et al., 2015) allow accurate assessment of erosion rates in the field or in an experimental (mesocosm) set-up (Wang et al., 2017; Beckers et al., 2020). For all these techniques, it is laborious and costly to obtain high frequency measurements in the field. *Fourthly*, the development of automatic in situ sensors, such as PEEP sensors (Lawler, 1991, 1992; Lawler et al., 2001) and SED (Sediment Elevation Dynamics) sensors (Hu et al., 2015a, 2015b, 2017, 2018; Willemsen et al., 2018) using light cells, allow continuous measurements of erosion and deposition at specific stations. When placed vertically into the sediment, they allow continuous measurements of relative elevation. When placed horizontally in the cliff edge, continuous measurements of the sediment-air interface allow detection of the marsh edge and thereby the movement of the cliff edge at high temporal resolution at one specific location. Thus, a distinction can be made between continuous saltmarsh edge erosion and episodic events of lateral saltmarsh erosion. Such automated sensor techniques have been applied to investigate the lateral erosion dynamics of river banks (e.g., Lawler et al., 1997), but, have to our knowledge, not been used to assess the lateral changes of saltmarshes.

In this article, we assess the occurrence, rates and potential drivers of lateral saltmarsh erosion by combining sensors with high spatial resolution (i.e., TLS) with sensors with high temporal resolution (i.e., SED sensors), thus obtaining a locally high spatio-temporal resolution. We hypothesize that a linear relationship between wave power and the cliff edge erosion rate should not only hold for long-term measurements (several months or years), but should also hold for short-term events (several hours, days), implying continuous retreat that intensifies with larger incident wave energy in retreating saltmarshes. Thus, it is expected that, based on wave energy and saltmarsh erosion measurements, an (extrapolation) prediction can be made about the rate of cliff retreat at severe storm conditions. We investigate (a) whether there is a consistent linear relationship between wave energy and the lateral saltmarsh erosion rate for a specific site, (b) whether there are critical

thresholds for wave energy to cause lateral saltmarsh erosion, and (c) whether mass failure (episodic slumping) occurs and cause non-linearity in the relationship between wave energy and the lateral saltmarsh erosion rate. We study this on a saltmarsh in the Westerschelde estuary, the Netherlands, using a combination of repeated terrestrial laser scans and continuous measurements using high resolution SED sensors and wave sensors, over a period of ca 2.5 years.

2. Study area

The study is carried out at Zuidgors, a temperate saltmarsh in the Westerschelde estuary, southwest Netherlands, near the village of Ellewoutsdijk (Fig. 1a, b). The Westerschelde is a turbid estuary (Eleveld et al., 2014) experiencing a macrotidal regime (spring tidal range at the nearby tide gauge station Hansweert is 5.8 m) and a seasonally varying, but low river discharge of ca 120 m^3/s (Cai et al., 2013). Continuous maintenance dredging and occasional capital dredging is carried out in the main channel of the Westerschelde estuary to maintain access to the port of Antwerp (e.g., Hu et al., 2017) and dredged material is disposed within the estuary. The saltmarsh vegetation at Zuidgors consists mainly of *Elymus athericus*, *Atriplex portulacoides*, *Aster tripolium*, and *Limonium vulgare*. The saltmarsh edge at Zuidgors is eroding with a distinct cliff edge of 60–80 cm in height (Fig. 1f), although there are also areas at Zuidgors without a cliff, where the saltmarsh vegetation is expanding or where pioneer saltmarsh vegetation has established in front of the cliff (van der Wal et al., 2008; Hu et al., 2015b), both west of the study site

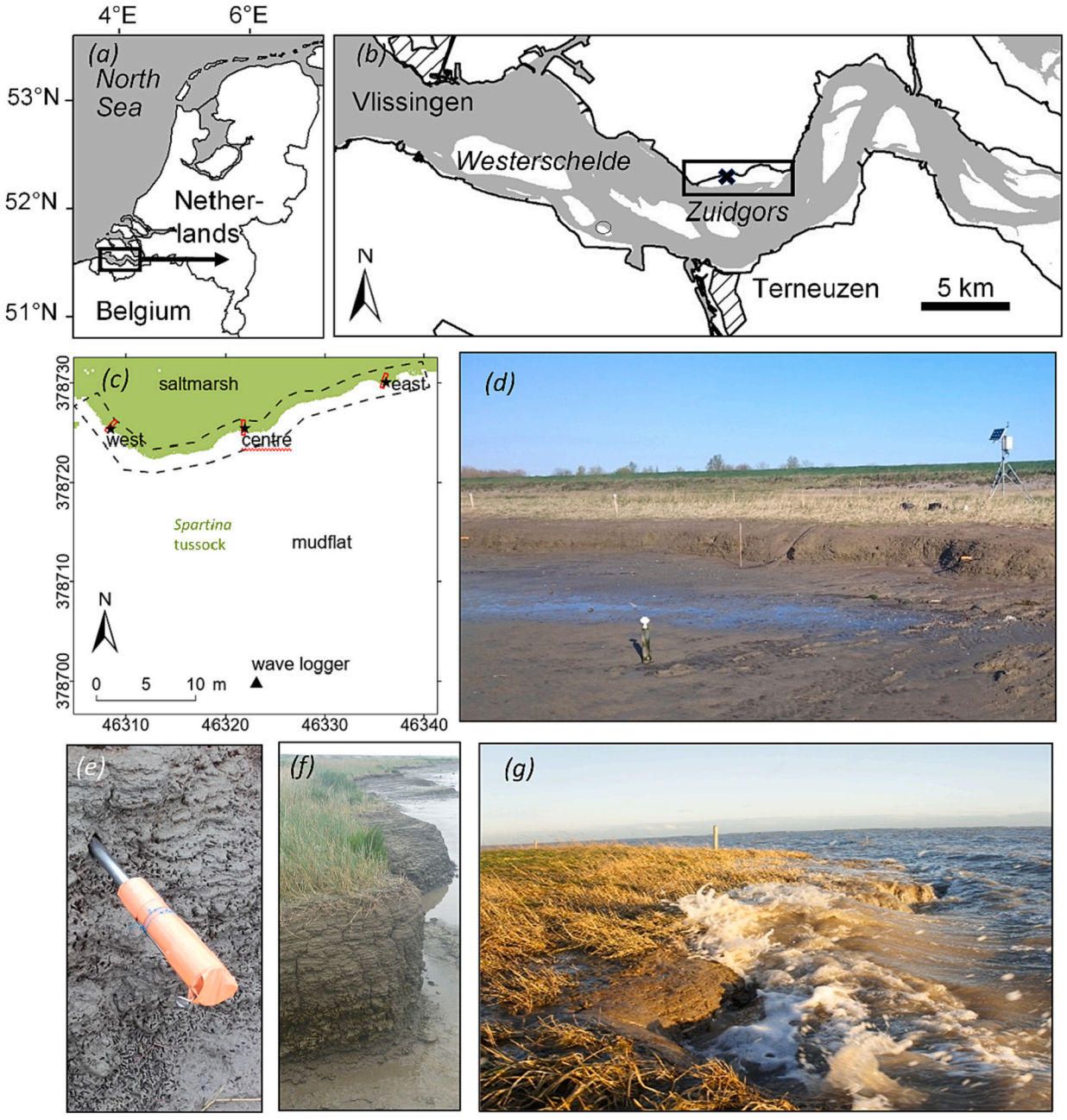

Fig. 1. (a) Westerschelde estuary, southwest Netherlands, and (b) Zuidgors, with study site marked with cross, (c) detail of the marsh edge (dashed polygon), with western, centre and eastern plots (rectangles with solid lines), location of the SED sensors (black stars) and wave sensor (black triangle), where saltmarsh area, shown in green, is based on a (25 cm resolution) TLS scan of October 2015, (d) part of the instruments deployed, also showing reflective TLS targets mounted on fixed poles, 19 Apr 2016, (e) a SED sensor, (f) a marsh cliff in Aug 2015 and (g) the study site during the gale of 23 Nov 2017. Photo (f) by Daphne van der Wal; photo (d), (e) and (g) by Jeroen van Dalen, NIOZ.

and in the east of Zuidgors. Zuidgors is exposed to the predominant southwesterly winds (van der Wal et al., 2008; Callaghan et al., 2010; Wang et al., 2017), and fronted by a mudflat that increases in size from west to east (Fig. 1b). Callaghan et al. (2010) measured average significant wave heights of 0.14–0.23 m on the tidal flat, and 0.02–0.03 m on the mature marsh, and average current velocities of 0.15–0.17 m/s on the tidal flat and 0.07 m/s on the mature marsh at Zuidgors. Significant wave heights at Zuidgors are highest between October to March (Callaghan et al., 2010). In a model study, average peak current velocities simulated for Zuidgors were found to be ca 0.4 m/s (ebb) to over 0.7 m/s (flood) for the mudflat at ca −2 m NAP (Mean Low Tide level), decreasing with elevation from the mudflat towards the marsh edge (De Vet et al., 2020).

The current study focuses on a stretch with an eroding cliffed marsh and adjacent upper mudflat. Three plots along the saltmarsh-mudflat transition, with slightly different exposure direction, were studied in detail (Fig. 1c).

3. Data and methods

3.1. Assessing vertical bed level and lateral marsh edge dynamics from TLS

Each month, in the period between 20 Oct 2015 and 25 Apr 2018, elevation of the upper mudflat and saltmarsh (for coverage, see dashed outline in Fig. 1c) was measured during low tide with a Riegl VZ400 TLS (Terrestrial Laser Scanner). Apart from monthly surveys, 2 events in autumn with predicted southwesterly storms were measured by TLS both before and after the event, i.e., the first event between 13 and 16 November 2015 and the second event between 20 and 24 November 2017 (Fig. 1g). The TLS scanner had a near-infrared wavelength, and the scanner was used with panorama 30 and high speed settings. Sites were surveyed from different angles by 5 scan positions to reduce occlusion effects. Still, the density of points was not homogenously distributed. We installed 5 fixed poles, on which reflection targets (with 5 cm diameter) were mounted during surveys; these were measured with RTK for referencing. Pre-processing was performed applying standard procedures in RiScan Pro software, using tie-points from the reflection targets to produce a point cloud for each TLS survey. We corrected for outlying air points, but not for the presence of vegetation. Note that this laser does not penetrate water and is not reflected from water, which resulted in missing data for parts of the tidal flats.

The sequential point data derived from the TLS scans were subsequently gridded in ArcGIS 10, with 1 cm pixel size; measurements were averaged per pixel for each time-step. Pixels without measurements (in the mudflat and saltmarsh) were assigned as no data pixel. In addition, an overview scan of the entire marsh was gridded with a 25 cm pixel size, applying the same procedure. Further processing was performed in R (software for statistical computing and graphics). To capture the bathymetric changes of the mudflat-saltmarsh transition in detail, three subareas ("plots") of ca 0.5 m in width and 1.5 m in length were defined (see location of the west, centre and east plots in Fig. 1c). Along the central length of each plot, a transect was defined, from which elevations were extracted at regular intervals of 1 cm to study profile changes. The position of the cliff edge for each profile was defined as the intersect with an elevation of 2.17 m NAP (which was roughly the elevation of the SED sensors in the cliff, see below). The lateral retreat in the plots (m day^{-1}) was calculated using the positions of the cliff in the TLS transect data. Additionally, elevation of the mudflat (saltmarsh base) was calculated as the average elevation over the 10 cm most seaward stretch of the 1.50 m long transect. Total marsh area was calculated of the entire stretch (Fig. 1c) for each raster, by counting pixels with an elevation of 2.17 m NAP or higher (defined here as marsh) and converting these to m^2 (thus ignoring no data pixels), while area changes of the entire marsh edge were expressed in m^2 day^{-1} (negative changes indicating loss and positive changes indicating expansion). For each of the 3 plots, and for the entire stretch, the mean elevation was calculated (ignoring no data pixels). Volumetric changes were calculated by subtracting the average elevation of two subsequent surveys and then multiplying the difference in elevation by the area of the plots; this was also done for the entire stretch.

Pearson correlations, respectively among the morphological metrics (i.e., states), and among the morphodynamic metrics (i.e., rates) from TLS data were analysed in R (with significance level α of 0.05). With this, we also tested for consistency of morphodynamics among the three plots as a measure for spatial correlation.

3.2. Assessing lateral marsh edge dynamics from SED sensors

SED sensors developed by NIOZ were used (Fig. 1e). The sensor is based on an array of 200 phototransistors, allowing detection of the air-sediment interface. The sensors measure position in the sediment with a resolution of 2 mm, although variation in position can be caused by scouring, and trembling of the sensor. The stand-alone SED sensors allow recording of multiple measurements per minute. Hu et al. (2015a) describe the instruments, approach and the accuracy of the SED sensor in detail, while Hu et al. (2017, 2018, 2021) examined vertical bed level changes on tidal flats using the SED sensors. Willemsen et al. (2018) developed a method to automatically process the position of the air-sediment interface for each tide, without the need for any contextual data, such as water levels or irradiance; this method is also applied in our paper to process the data. The SED sensor obtains data with multiple sensitivities, when daylight is sufficient and the sensor is not inundated, and these were all used to increase data coverage during dusk and dawn. Data were subsequently averaged per day. In our case, three SED sensors were placed *horizontally* in the marsh edge. The sensors were placed in Oct 2015 just east of the detailed plots west, centre and east, respectively (Fig. 1c), and were replaced in March 2017. The position of the sensors was measured with RTK (see Electronic Supplementary Material 3). Sensors needed to be pushed further into the cliff occasionally, after read-out. Read-out of the sensors (see Electronic Supplementary 2) meant a reset, after which the time-series were aligned with the previous time-series. In the last period of each series, scour holes of the point where the SED sensors were placed into the cliff caused erroneous measurements, as light penetrated the cliff edge. By the end of the second period, the SED sensor at the centre location was found to be dislodged. The SED sensor in the western station malfunctioned in the second period.

Pearson correlations among the time-series of cliff positions from the 3 SED sensor stations were analysed in R (with $\alpha < 0.05$ significance level) to test for consistency of the time-series at the 3 stations. The time-series of the cliff positions from the SED sensors were further analysed using a breakpoint analysis to detect structural changes (such as erosion events) with the package "strucchange" in R (Zeileis et al., 2002; Zeileis et al., 2003). The breakpoints (i.e., last observation in a segment) and corresponding breakdates (i.e., positions of the breakpoints) are calculated by minimizing the residual sum of squares in linear (time series) regression analyses (Zeileis et al., 2002). The analyses were done in two parts: period I corresponding to the first set of instruments from 20 Oct 2015 until 1 March 2017 and period II corresponding to the second set of instruments from 1 March 2017 until 28 April 2018. The western transect had too few data in period II to perform the breakpoint analysis.

3.3. Measurements of hydrodynamics and wind

A pressure transducer sensor (OSSI-010-003B) continuously logged wave conditions and water depth in front of the cliff, ca 50 m seaward on the mudflat, at ca 1.7 m NAP (where NAP is the Dutch datum, approximately mean sea level) (see Electronic Supplementary Material 13 for exact location). The sampling frequency of the wave logger was set to 10 Hz, sampling the first 7 min of each 15 min interval. Significant wave height (Hs, in m) and significant wave period (Ts, in s) were calculated

from spectra of pressure data for each burst. The instrument was read out and replaced regularly. Daily average values for Hs and Ts were obtained, considering all 15 min intervals on a day during inundation (cf. Fig. 7). One extreme outlier was removed from the wave data (burst 4 Oct 2017 8h31, incoming tide, with water depth D = 0.05 m, and Hs = 3.2 m; this did not affect Table 3). Calculation of the wave energy flux per unit wave-crest length, or wave power P, was adapted from Guillou (2020). In our paper, the wave power Ps (in W/m) was assumed to scale with daily values of Hs and Ts as follows:

$$Ps = \frac{1}{64\pi}\rho g^2\, Hs^2\, Ts \quad (1)$$

where ρ is the density of water and g is the gravitational acceleration (9.81 m/s^2). In our study, ρ is taken as 1019 kg/m^3, assuming a mean salinity of 25 and a mean temperature of 15 °C, and based on the 1 atm equation for sea water in Millero and Poisson (1981). The period of time when the logger was flooded with water (water depth D > 0) was taken as inundation duration (I) in hours; this is also approximately the duration that the base of the saltmarsh was flooded. This quantity I was multiplied by Ps to obtain the wave energy (Wh/m). The logger was flooded when the water level was close to the 1.85 m NAP of the upper bare mudflat, cq. the base of the saltmarsh. Average and maximum water depth D (in m) during inundation were also retrieved per day. If there was no flooding of the logger during a day, a value of 0 was assigned to all hydrodynamics variables for that day. The logger was not operational in the period 27 Feb 2016 until 20 Apr 2016; hydrodynamic variables in this period were assigned as "no data".

Meteorological data were obtained from KNMI (Royal Netherlands Meteorological Institute) for nearby station Hansweert (located 3.998° East, 51.447° North) with mean daily wind direction ("DDVEC"), mean daily wind speed ("FG") and maximum hourly wind speed ("FHX") for each day. According to KNMI, storm is defined as hourly wind speeds of 20.8 m/s or higher. Additional 10 min scalar mean wind velocities corrected for 10 m above sea level ("WC10" data) were obtained from the Hydro Meteo Centrum of Rijkswaterstaat for Hansweert to categorize winds conform Beaufort scale, where gales (8 Beaufort) have at least one mean 10 min wind speed of 17.2–20.7 m/s, strong gales (9 Beaufort) of 20.8–24.4 m/s and storms (10 Beaufort) of 24.5–28.4 m/s.

The morphodynamic metrics from the TLS measurements were related to the average daily hydrodynamic and meteorological variables for each period using a Pearson correlation (with α = 0.05 significance level).

3.4. Sampling of sediment properties

Sediment samples were taken with a syringe from which the nozzle was cut off (3 cm depth, volume of 19 cm^3) in spring 2017 from the cliff edge face, at different heights above the mudflat surface (i.e., 10 cm intervals). They were collected close to the 3 SED sensors at location west, centre and east, respectively. In the NIOZ laboratory, samples were freeze-dried, and subsequently analysed with a Malvern 2000 laser particle sizer to obtain mud content (fraction <63 μm) and median grain-size (d50, in μm), and dry bulk density (in g/cm^3). Average values of the sediment properties were calculated from all samples of each cliff edge location, for all samples except for the lowest sample of each cliff edge, i.e. the saltmarsh base, and for the saltmarsh base only. The sediment properties were related to the vertical and lateral erosion rates at the western, centre and eastern plot.

4. Results

4.1. Vertical bed level and lateral marsh edge dynamics from TLS

TLS scans reveal lateral cliff retreat over the years along the entire stretch of the marsh edge, including the detailed transect plots in the west, centre and east (Figs. 2 and 3; Electronic Supplementary Materials 3–7; photos Electronic Supplementary Materials 8–9). The detailed cross-sections obtained from TLS (Fig. 4) confirm a lateral retreat of the marsh edge at all 3 transect plots, and a gradual lowering of the marsh surface. Particularly from autumn 2017 onwards, the marsh face in the 3 plots appears irregular (Fig. 4). The TLS surveys revealed substantial lateral retreat and deposition of slumped material on the mudflat between 5 Sep 2017 and 4 Oct 2017 in particularly at the centre and western transect (Fig. 4; Electronic Supplementary Materials 4–6). The lateral erosion rate of the marsh edge at the 3 plots was relatively low between Nov 2017 and Jan 2018 (Fig. 4). The base of the saltmarsh edge persisted, resulting in a terraced surface (Fig. 4). However, by Apr 2018, the saltmarsh in the 3 plots had largely been converted into mudflat (Figs. 2 and 4).

In the beginning of the survey period, the saltmarsh-mudflat system overall lost sediment (less sediment volume) in the three plots (Fig. 4). The elevation of the upper mudflat temporally increased at all three plots at the beginning of 2017 (Electronic Supplementary Material 10), while erosion of the cliff and saltmarsh surface continued (Fig. 4). The final cross-sections and TLS collected in Apr 2018 showed that the mudflat had accreted in early 2018 in particularly in the west, in parallel with continued lateral saltmarsh retreat (Fig. 4; Electronic Supplementary Materials 3–6).

Time-series of the entire stretch under study show a gradual loss of saltmarsh area (Fig. 5a). Pronounced events in lateral erosion in Jan/Mar 2017 and in Sep/Oct 2017 were observed in the centre transect (Fig. 5c; Electronic Supplementary Material 5). In the western transect, the changes in Sep/Oct 2017 and Jan/Apr 2018 were also apparent (Fig. 5c; Electronic Supplementary Material 4), as was an event in May/July 2017 (Fig. 5c).

While average elevations from TLS in the three transect plots were highly correlated (Fig. 5b, Electronic Supplementary Material 11), volumetric *change* was only significantly correlated between specific locations, i.e., between the western and the centre plot, and between the entire stretch and the western and centre plot (Table 1). The cliff position obtained from TLS was also strongly correlated among the three transects, with all transects showing retreat (Fig. 5c; Electronic Supplementary Material 11). Lateral *change* in the position of the cliff edge at the 3 transects was not consistent: the rates in the western and eastern transect were positively correlated, while the rates in the centre and eastern transect were negatively correlated (Table 1). Thus, while all transects suffered from erosion, there was only weak spatial correlation of the volumetric changes and lateral erosion rate along the three different locations of the marsh edge. Moreover, volumetric change at the saltmarsh-mudflat interface and lateral changes in cliff position did only correspond at the western and eastern transect; the centre transect had a negative correlation between vertical and lateral change (Table 1).

4.2. Lateral marsh edge dynamics from SED sensors

The SED data allowed continuous measurements of the cliff retreat. They confirmed the mostly continuous lateral erosion rates of the cliff edge (Fig. 6). In the western and eastern transects, gradual (linear) erosion took place, and rates were very closely linked between these two stations (r = 0.90 for the entire period until 25 Apr 2018, see also Electronic Supplementary Material 12, and r = 0.94 for the first period in 2015 and 2016, all $P < 0.001$, note there were limited data in the second period for the western SED sensor). The resemblance between the lateral erosion rates of the eastern and western transects from SED sensor data was also seen in the TLS data (cf. Figs. 5c and 6; Table 1).

Nevertheless, the SED sensor time series showed periods with distinct lateral erosion rates where segments with a distinct trend are separated by breakdates (i.e., dates of the breakpoints) (Fig. 6). A number of breakdates roughly corresponded to the timing of replacement or re-set of the SED sensors and may hence be a measurement artefact (Electronic Supplementary Material 2). For example, in Sep and

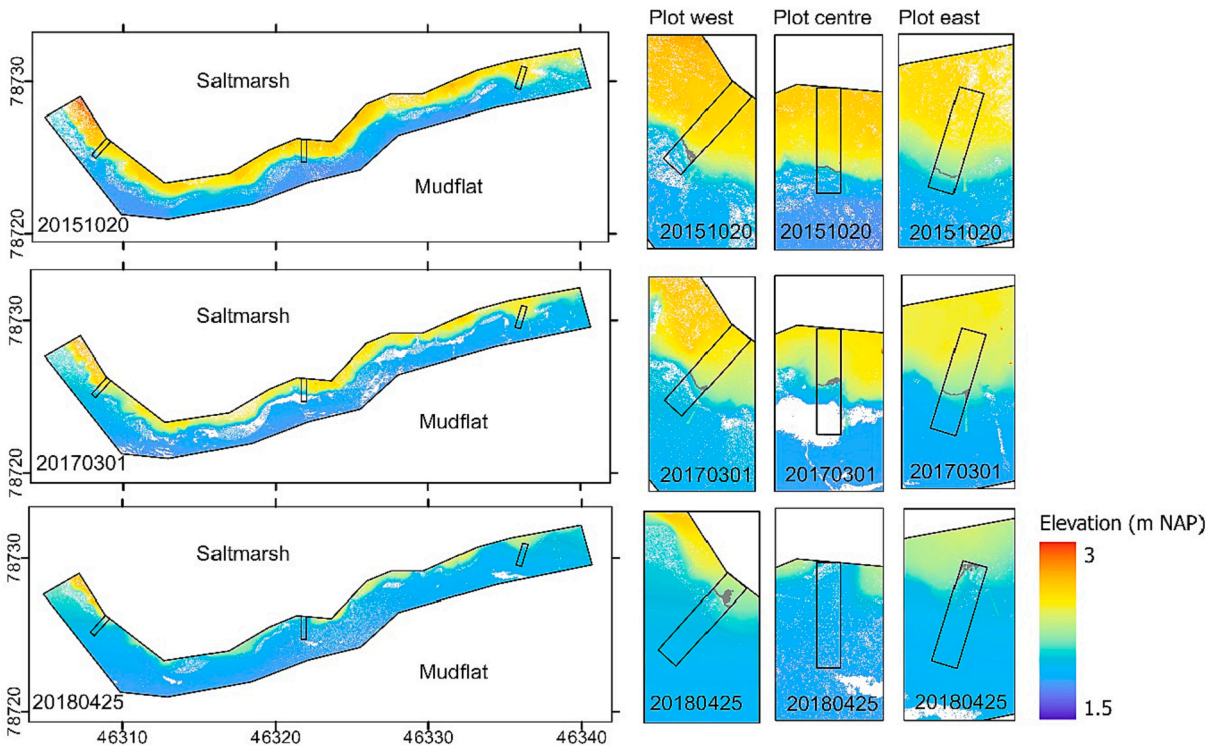

Fig. 2. Digital Terrain Models from Terrestrial Laser Scan data for 20 Oct 2015, 1 March 2017 and 25 April 2018, with 1 cm resolution grids. Three transect plots are shown in detail in the right hand side panels; these plots are located close to the SED sensors (see Fig. 1c for locations). The dark grey line in the detail plots indicates the most seaward contour of 2.17 m NAP, representing the marsh edge.

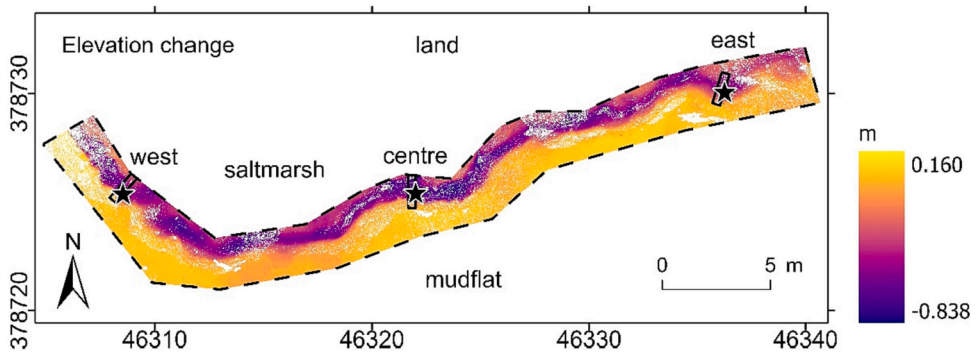

Fig. 3. Elevation change between 20 Oct 2015 and 25 Apr 2018 from TLS data of the marsh edge from 1 cm resolution grids. Positive values denote sedimentation, negative values denote erosion. Plots are indicated with solid black rectangles, and locations of the SED sensors are shown as stars.

Oct 2017 the SED sensors were pushed in (after substantial lateral retreat), and hence the substantial lateral change as observed in the TLS data may not have been reflected well in the SED time-series. However, there were additional breakdates in the time-series of the position of the marsh edge for one or more sensor locations, such as those in Dec 2015, June and August 2016 and June and July 2017 (Electronic Supplementary Material 13). For example, the breakdate in June/July 2017 showed a distinct increase in the lateral erosion rate in both the centre and eastern SED location (Fig. 6). In Nov 2017, a period with little change was detected by particularly the centre SED sensor (Fig. 6); this mimicked the reduction of changes in the lateral position of the cliff observed from TLS (Fig. 5c).

4.3. Hydrodynamics and wind as drivers of changes of the marsh cliff edge

Two events with southwesterly winds were observed in detail, 13–16 Nov 2015 (maximum hourly wind speeds of 17 m/s and 10 min wind speeds of up to 17.7 m/s at station Hansweert, 8 Beaufort, gale force winds) and 20–24 Nov 2017 (maximum hourly wind speeds of 16 m/s and maximum 10 min wind speeds of up to 17.5 m/s, 8 Beaufort, gale force winds), with TLS scans performed both before and after the event. Particularly during the period with the gale in Nov 2015, values for water depth, inundation duration, wave height, power and energy and wind speed were high and the wave period was intermediate, while during the period of the event in Nov 2017, particularly values for inundation duration and wind speed were high (Fig. 7). The Nov 2015 gale coincided with an apparent temporary increased loss of total saltmarsh area from TLS data (Fig. 5a) followed by an apparent gain in the next period. In addition, there was a limited decrease in elevation of the marsh-mudflat area (e.g. western transect in Fig. 6b) and very limited or no increase in lateral erosion (Fig. 5c). The event in Nov 2017 was associated with a limited loss of marsh area from TLS data (Fig. 5a), lowering of overall elevation, particularly at the centre transect (Fig. 5b)

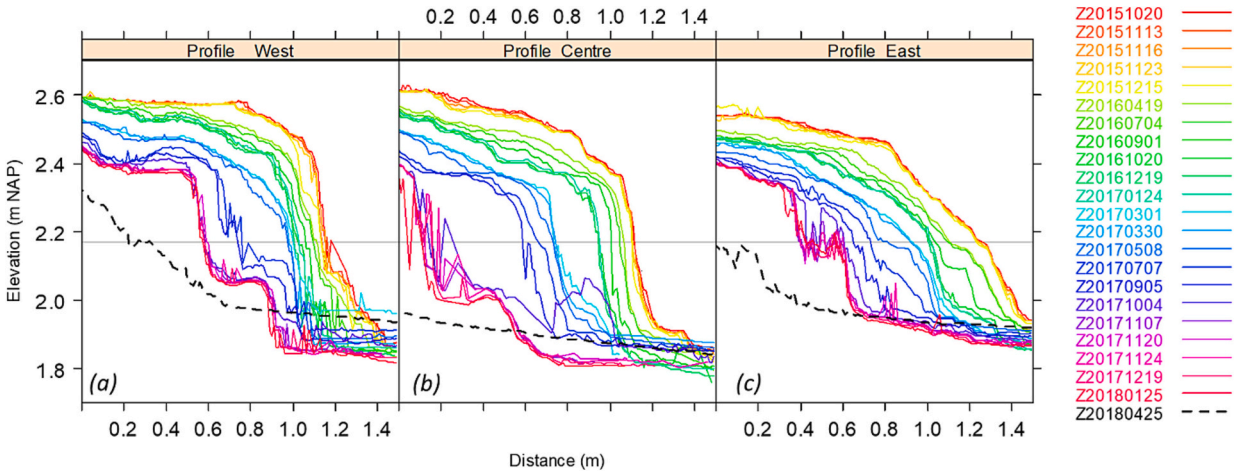

Fig. 4. Elevation changes from TLS data at the mudflat-saltmarsh transition for the transect (a) west, (b) centre and (c) east. Profiles are denoted with their date (elevation Z yyyy-mm-dd); the highest red line is the oldest (20 Oct 2015) and the black dotted line is the latest (25 Apr 2018) measurement. The position of the marsh edge is defined as the intersection of a profile with 2.17 m NAP (horizontal grey line).

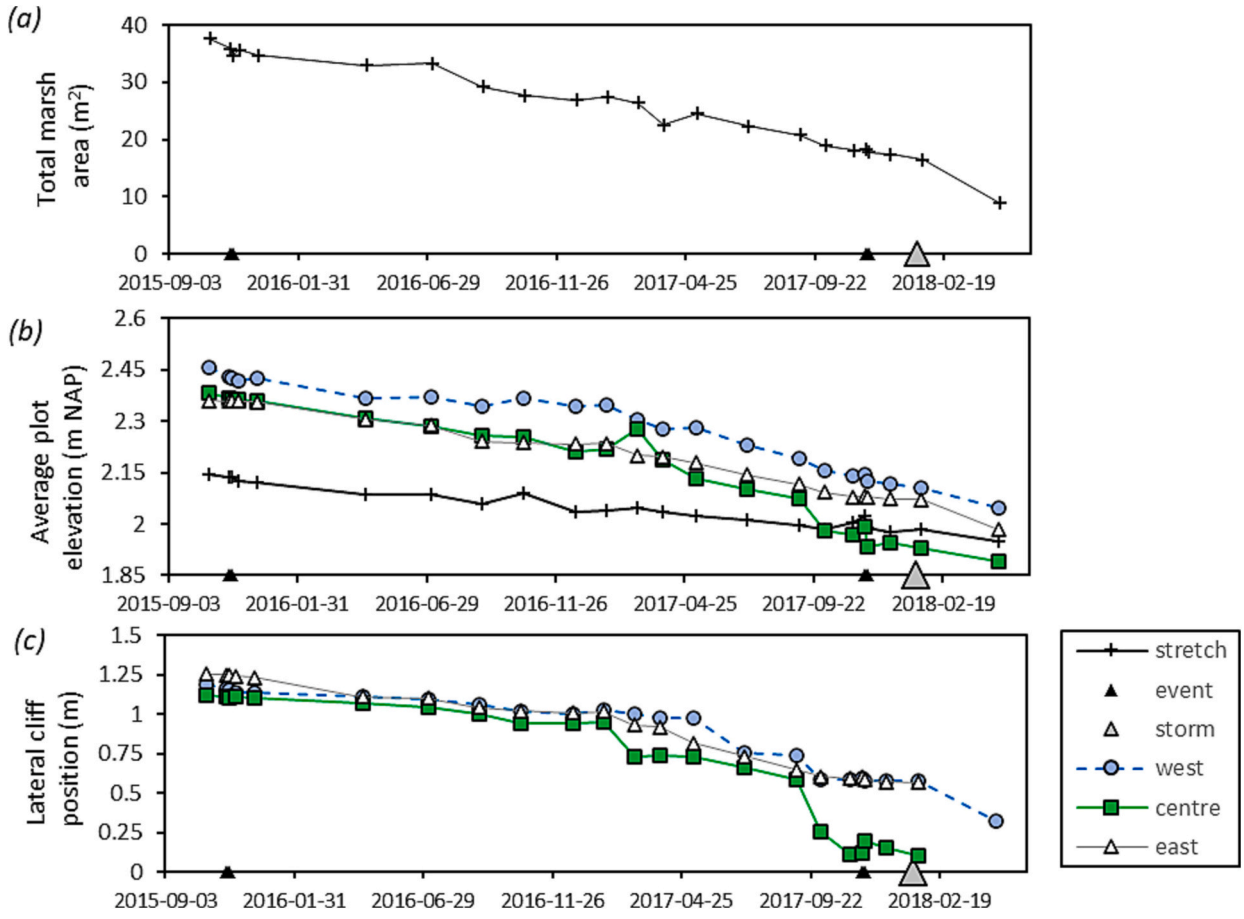

Fig. 5. Time-series derived from TLS of (a) total marsh area, (b) average elevation of three plots at the saltmarsh-mudflat transition and the entire saltmarsh-mudflat stretch, and (c) lateral position of the cliff (intersection of profile with 2.17 m NAP). Black triangles indicate the timing of two gale events (8 Beaufort) with TLS measurements before and after the wind event (between 13 and 16 Nov 2015 and between 20 and 24 Nov 2017, respectively), and large grey triangle indicate the strong gale/storm (9 Beaufort) recorded on 18 Jan 2018 (see Fig. 7 for meteorological conditions).

and an apparent progression of the marsh at the centre transect (Fig. 5c). The effect of the two events was not observed in the SED sensor data of the 3 plots (Fig. 6). On 18 Nov 2018, a storm (maximum mean hourly wind speeds of 23 m/s and mean 10 min wind speed of up to 24.4 m/s at Hansweert, 9 Beaufort, strong gale) was recorded (Fig. 7h); without noticeable increased morphodynamics, neither in the TLS data (Fig. 5) nor in the SED sensor data (Fig. 6).

As expected, significant wave height was positively correlated with inundation duration, water depth, wave power and energy, as well as average and maximum hourly wind speed, and had a significant

Table 1
Pearson correlations of metrics derived from TLS measurements, i.e., changes in marsh area (m^2/day) and total volumetric change of the saltmarsh-mudflat interface (m^3/day), average volumetric change per day (m^3/day) in the western, centre and eastern plot and change in lateral position of the cliff per day (m/day) in the western, centre and eastern transect. Number of periods $N = 21$ for correlations involving cliff position in the centre and eastern plot (no data available for the final period) and $N = 22$ for all other correlations. Significance is noted by stars, **** is $P < 0.0001$, *** is $P < 0.001$, ** is $P < 0.01$ and * is $P < 0.05$ and NS is not significant.

	Volumetric change in plots			Lateral change in cliff position		
	West	Centre	East	West	Centre	East
Marsh area change, total stretch	NS	NS	NS	NS	NS	NS
Volumetric change, total stretch	0.87****	0.95****	NS	NS	−0.82****	0.79****
Volumetric change in plots						
West		0.85****	NS	0.58**	−0.58**	0.76****
Centre	0.85****		NS	0.44*	−0.74***	0.77****
East	NS	NS		NS	NS	0.46*
Lateral change in cliff position						
West	0.58**	0.44*	NS		NS	0.45*
Centre	−0.58**	−0.74***	NS	NS		−0.51*
East	0.76****	0.77****	0.46*	0.45*	−0.51*	

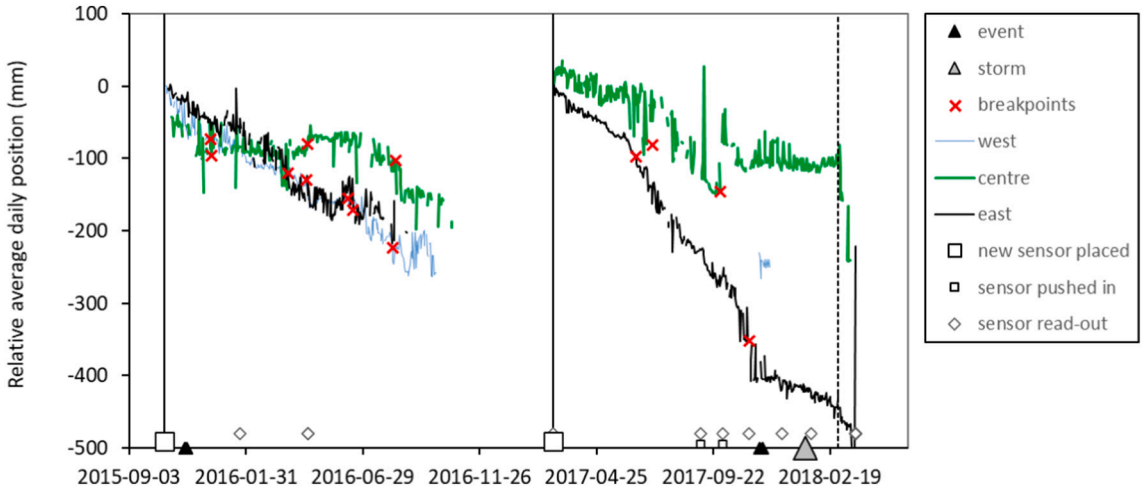

Fig. 6. Position of the cliff from SED sensors (relative position in mm), at location west, centre and east. Vertical lines and large open rectangle symbols at the bottom of the graphs indicate a new set of sensors (and reset of relative position), small open rectangles at the bottom line indicate time when a sensor is pushed into the cliff (corrected for in relative position) and open diamonds indicate a read-out/reset (corrected for in relative position). Closed triangles indicate the two events investigated in detail, whereas a strong gale/storm detected at station Hansweert is indicated with a large grey triangle (see Fig. 7 for meteorological conditions). Breakdates, delineating segments with distinct trends, as identified by the structural change analysis, are indicated as red crosses for each sensor (see also Electronic Supplementary Material 13). The dashed vertical line is at 1 March 2018.

negative correlation with wave period (Table 2). In general, the morphodynamics obtained from TLS had only weak or insignificant correlations with hydrodynamics and wind (Table 3; Electronic Supplementary Material 14). Significant negative correlations were found between the changes in the area of the entire marsh of the study and all hydrodynamic and wind metrics, except for wave period (Table 3). Volumetric changes of the entire saltmarsh-mudflat interface did not correlate significantly with hydrodynamics, except for a significant negative correlation with inundation duration and average wind speed (Table 3; Electronic Supplementary Material 14). We found a significant negative correlation of volumetric change with inundation duration and wind speed for the western and centre plots, but not the eastern plot, as well as a significant, unexpected *positive* correlation of volumetric change with water depth, wave height, wave power and wave energy for the eastern plot. The lateral rates of marsh edge erosion from TLS at the three detail plots were not significantly correlated with hydrodynamics or winds (all $P > 0.05$).

4.4. Sediment properties as drivers for resistance of the marsh cliff edge

The sediment of the saltmarsh edge was composed of sandy mud or mud (Fig. 8). Cliff faces were coarsest at the surface, with particularly in the cliff face in the western plot also coarser material at the base, while bulk density decreased with depth (Fig. 8). Lateral retreat rates, as obtained from TLS, were slowest for the plot with the coarsest cliff edge and marsh base (western transect) and fastest for the plot with the finest cliff edge and intermediate cliff base (centre transect) (Electronic Supplementary Material 15). However, lowering of elevation was slowest in the plot with the intermediate marsh cliff and finest marsh base (eastern transect), and fastest in the plot with the finest marsh edge and intermediate marsh base (centre transect) (Electronic Supplementary Material 15).

5. Discussion

Our results at Zuidgors point to a mostly gradual erosion process of the marsh edge. Indeed, in absence of storms, lateral erosion continued. Lateral marsh cliff edge erosion took place at all 3 plots studied in detail. Correlation among erosion rates as obtained from sequential TLS scans at these 3 transect plots along the marsh edge was weak (cf. Table 1), pointing to weak correlation in space between erosion events, and hence local variations. Nevertheless, the SED sensors showed a remarkable resemblance in very gradual, linear erosion rates between two stations in 2015 and 2016, and synchronous changes in the rate of erosion between sensors in some periods (cf. Fig. 6). In the case of Zuidgors, it appears that moderate energy events can already induce lateral erosion

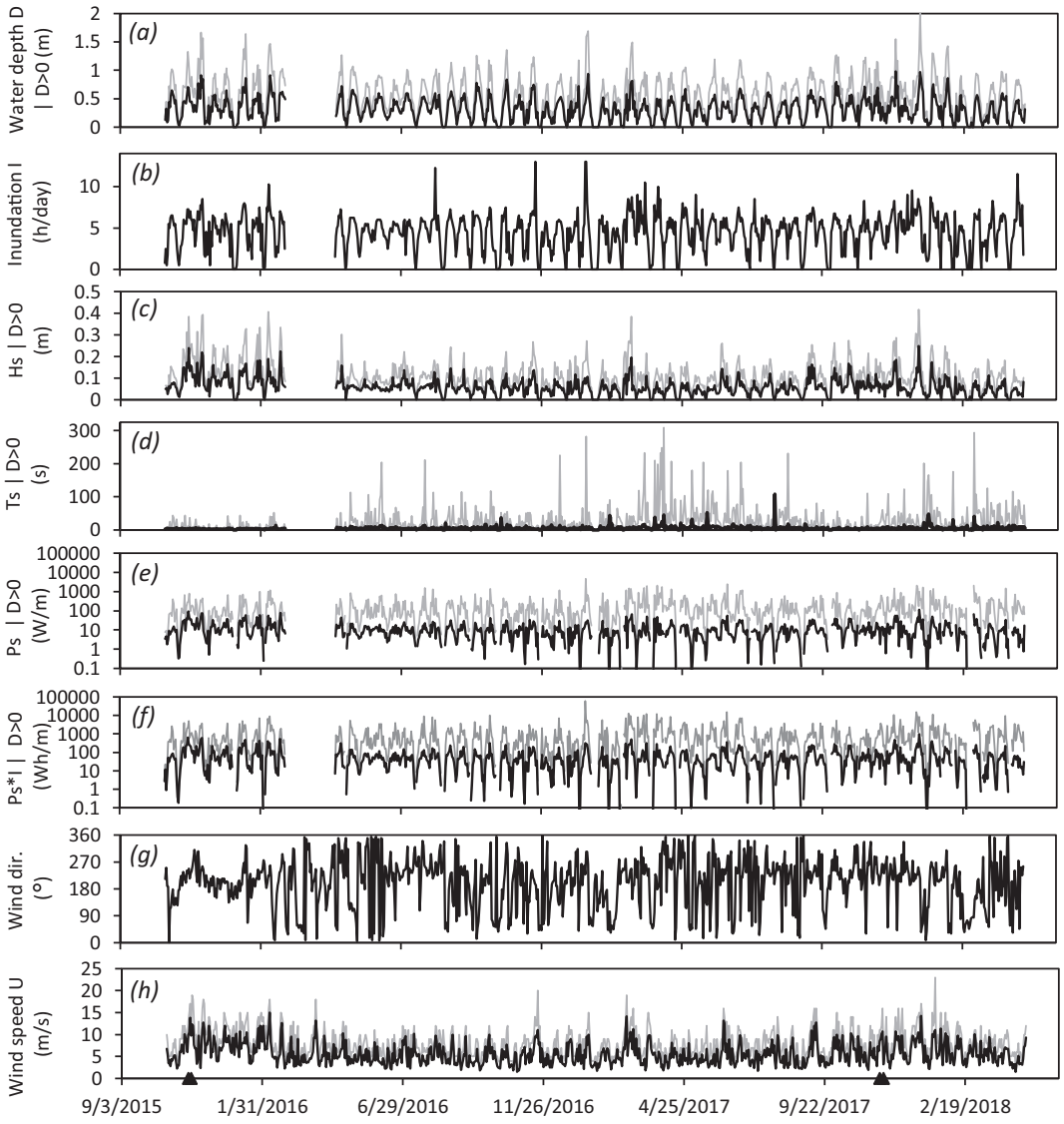

Fig. 7. Time-series of hydrodynamics at the upper mudflat, with (a) water depth during inundation, (b) daily inundation duration, (c) significant wave height, (d) significant wave period, (e) wave power, on a logarithmic scale, (f) wave energy on a logarithmic scale, (g) wind direction and (h) wind speed. Black lines are daily average and grey lines are daily maximum values; for (h) black lines are daily average hourly and grey lines are daily maximum hourly measurements. Two events are marked with black triangles, the first in 13–16 Nov 2015 (hourly wind speed up to 17 m/s, 10 min scalar wind speed up to 17.7 m/s, gale, 8 Beaufort), the second in 20–24 Nov 2017 (hourly wind speed up to 16 m/s, 10 min scalar wind speed up to 17.5 m/s, gale, 8 Beaufort). A storm (mean hourly wind speed of up to 23 m/s, storm as defined by KNMI; and 10 min scalar wind of up to 24.4 m/s, strong gale, 9 Beaufort) is indicated with a large grey triangle. No hydrodynamic data were available for spring 2016.

Table 2
Pearson correlation matrix of inundation duration (I, hours), average water depth (D, m), significant wave height (Hs, m), significant wave period (Ts, seconds) and derivatives average significant wave power or energy flux (Ps, W/m) and energy Ps * I (Wh/m), average hourly wind speed (U, m/s) and average maximum daily hourly wind speed (Umax, m/s) at station Hansweert, for N = 22 periods. Significance is noted by stars, **** is $P < 0.0001$, *** is $P < 0.001$, ** is $P < 0.01$, * is $P < 0.05$ and NS is not significant.

	I	D	Hs	Ts	Ps	Ps * I	U	Umax
I		0.62**	0.71***	NS	0.76****	0.76****	0.88****	0.89****
D	0.62**		0.93****	−0.51*	0.90****	0.88****	0.66***	0.68***
Hs	0.71***	0.93****		−0.57**	0.96****	0.94****	0.83****	0.85****
Ts	NS	−0.51*	−0.57**		NS	NS	−0.45*	−0.43*
Ps	0.76****	0.90****	0.96****	NS		1.00****	0.81****	0.82****
Ps * I	0.76****	0.88****	0.94****	NS	1.00****		0.81****	0.82****
U	0.88****	0.66***	0.83****	−0.45*	0.81****	0.81****		0.99****
Umax	0.89****	0.68***	0.85****	−0.43*	0.82****	0.82****	0.99****	

Table 3
Pearson correlations between inundation duration (I, hours), average water depth (D, m), significant wave height (Hs, m), significant wave period (Ts, seconds) and derivatives average significant wave power or energy flux (Ps, W/m) and energy Ps * I (Wh/m), average hourly wind speed (U, m/s) and average maximum hourly wind speed (Umax, m/s) at station Hansweert, and morphodynamic metrics derived from TLS, i.e., total marsh area change (m^2 day^{-1}) and total volumetric change (m^3 day^{-1}), and cliff position (m day^{-1}). Number of periods N = 21 for correlations involving cliff position in the centre and eastern plot (no data available for the final period) or N = 22 for all other correlations. Significance is noted by stars, ** is P < 0.01 and * is P < 0.05, and NS is not significant.

Variable	Marsh area change	Volumetric change				Lateral change in cliff position		
	Total stretch	Total stretch	West	Centre	East	West	Centre	East
I	−0.52*	−0.43*	−0.49*	−0.45*	NS	NS	NS	NS
D	−0.54**	NS	NS	NS	0.59**	NS	NS	NS
Hs	−0.51*	NS	NS	NS	0.52*	NS	NS	NS
Ts	NS	NS	NS	NS	NS	NS	NS	NS
Ps	−0.62**	NS	NS	NS	0.53*	NS	NS	NS
Ps * I	−0.65**	NS	NS	NS	0.53*	NS	NS	NS
U	−0.58**	−0.46*	−0.57**	−0.44*	NS	NS	NS	NS
Umax	−0.52**	NS	−0.52*	NS	NS	NS	NS	NS

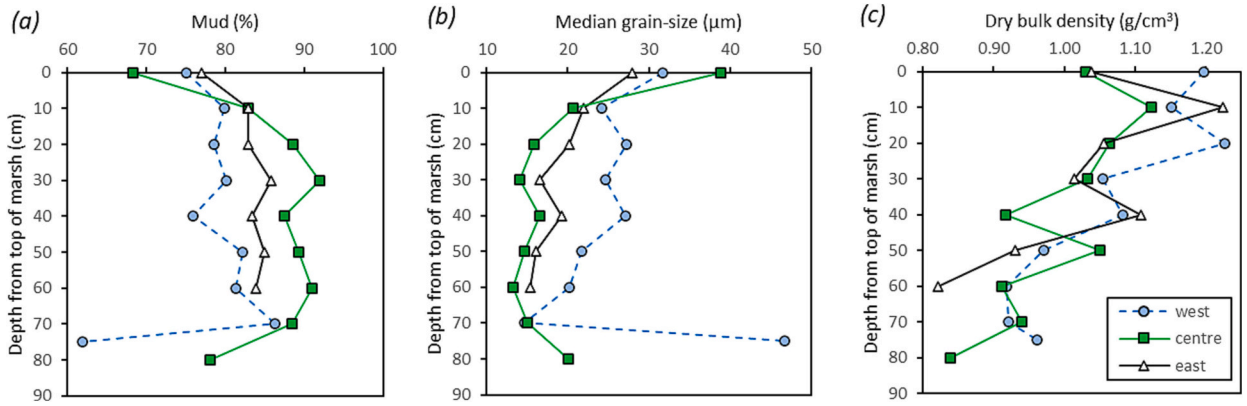

Fig. 8. Sediment samples of the cliff face at the location of the SED sensors (sampled on 23 Jan 2017). Upper sample (0 cm depth) is the marsh surface (saltmarsh plateau), lowest sample is the saltmarsh base.

of the marsh cliff edge.

A large body of literature exists that relate lateral erosion rates to wave energy (e.g., Schwimmer, 2001; Karimpour et al., 2016; Leonardi et al., 2016b; Tommasini et al., 2019), although McLoughlin et al. (2015) found a stronger relationship between wave energy flux and volumetric erosion rates than with lateral erosion rates. Research in Galveston, Texas employed TLS over one year to retrieve the erosion rates of a saltmarsh edge and found a very strong correlation with wave energy (Huff et al., 2019). Leonardi et al. (2016a, 2016b) found a linear increase between lateral saltmarsh erosion and wave power. We hypothesized that a linear relationship between cliff edge erosion and wave power should not only hold for long-term measurements, but should also hold for short-term changes, implying continuous retreat that intensifies during larger incident wave energy. However, water depth may additionally regulate hydrodynamic forcing on the bottom sediment (bed shear stress). We found a weak correlation between loss rate of saltmarsh area from TLS and inundation duration and wave and wind action for the entire stretch under study (Table 3). Additionally, we only found a significant negative correlation between overall volumetric sediment change of the mudflat-saltmarsh stretch and average inundation duration and wind speed, while correlations varied or were not significant for the three detail plots (cf. Table 3). No significant correlations were found between hydrodynamics and the local lateral erosion rates, neither from TLS (Table 3) nor from the SED sensors (cf. Fig. 6).

The number of missing pixels (see Electronic Supplementary Materials 4–6), and the vegetation likely biased our morphodynamic metrics from TLS surveys, particularly when the period between consecutive surveys was small (e.g., before and after the wind events). This might explain, for example, that we detected overall loss of total saltmarsh area in 13–16 Nov (wind event), followed by gain in 16–23 Nov 2015 (cf. Figs. 4 and 5; Electronic Supplementary Material 14), while the edge of the saltmarsh continued to retreat. Regardless, the long-term erosional trend indicates that erosion under common fair-weather conditions outweigh effects of incidental strong winds on erosion.

Our results suggest that erosion at our site is inherently linked to conditions such as the position of the mudflat-saltmarsh system in the tidal frame. On a longer time-scale, van der Wal et al. (2008) demonstrated for this site that the erosion rate is correlated with the width of the intertidal foreshore. In this case, dredged sediment was disposed west of this site in the 1990s, feeding the mudflat, and slowing down the saltmarsh retreat rate (Hu et al., 2017). Hu et al. (2017) concluded from SED measurements of the vertical movements of the mudflat that tidal currents were more important than waves in this study area, attributing the erosional trend at the mudflat to a combined effect of hydrodynamic forcing and reduced sediment supply. Hu et al. (2018) found that even during constant hydrodynamic forcing, the tidal flat was erosive. In our study, we demonstrate that this erosive trend extends to the saltmarsh, and examine the link between the mudflat and the saltmarsh. Our plots were overall erosive, that is, erosion of the saltmarsh was not balanced by deposition of sediment on the higher mudflat. Nevertheless, the deposition of sediment on the higher mudflat, as well as the increase in mudflat width at the landward side, may have induced reduced erosion rates of the cliff, as waves on this higher mudflat would have had less energy. Once a marsh cliff edge is induced due to a discontinuity in sediment stability (Bouma et al., 2016), lateral erosion continues, until the foreshore is sufficiently wide to attenuate waves and reduce sediment dynamics and pioneer saltmarsh can (re-)establish (Bouma et al., 2016; Cao et al., 2018). This re-establishment buffers the waves further, thereby reducing erosion of the marsh plateau behind it (Van de Koppel et al., 2005; van der Wal et al., 2008; Wang et al., 2017; Evans et al.,

2019; Schuerch et al., 2019; Willemsen et al., 2018). In the stretch of marsh in our study site, re-establishment of vegetation was not yet occurring, although in between the western and centre transect, a patch of *Spartina* spp. was already present and in nearby stretches, the pioneer vegetation expanded.

In our study, we observed spatial variation in erosion rates among transects. Bendoni et al. (2019) found in model simulations that marsh edges are steeper in mud than in sand, and maintain their shape better while retreating. Wang et al. (2017) showed in a mesocosm wave tank experiment with sediments from the saltmarsh cliff at several sites in the Westerschelde estuary that the volume loss of sediment during waves increased with a decrease of sediment grain-size, where volume loss was especially high when median grain-size was below 50 μm. Similar results were found for Venice lagoon (Lo et al., 2017), while on the island of Schiermonnikoog, Marin-Diaz et al. (2021) found a more complex relation between erodibility and mud content. In our case, the differences in sediment grain-size between the 3 plots might have been relatively small, and although the fastest erosion rates were observed at the marsh face with the finest sediment (cf. Electronic Supplementary Material 15), the relationships between sediment characteristics of the cliff edge and base and morphodynamic change were not unambiguous. Cracks in the surface sediment (that were observed on various days, cf. photos in Electronic Supplementary Material 9 of the centre transect) combined with laminae formed during deposition may have facilitated erosion of aggregates. Adriaens et al. (2018) report amounts of e.g., smectite clay minerals in the Westerschelde sediments; such sediments have swelling/shrinking properties.

Wang et al. (2017) found that in the Westerschelde estuary, the effect of erodibility was subordinate to the effect of exposure to the dominant wind direction on lateral erosion. While the marsh at Zuidgors is subject to the predominant southwesterly winds/waves, some local variation may also be explained by contrasting exposure to waves, with the western and eastern plot facing southwest and the centre plot facing southwards. Moreover, the presence of a patch of *Spartina* on the mudflat in between the western and centre plot may have resulted in local wave dampening.

The role of vegetation in influencing lateral rates of cliff erosion was not investigated in detail in this study. Vegetation properties of the marsh edge, such as aboveground biomass and root density, can enhance the stability of the saltmarsh edge (De Battisti et al., 2019). In places with vegetation, vertical bed level variability may also be limited (Willemsen et al., 2022). Vegetation occurrence is limited by a sum of stress from inundation and bed level change, where any excess of bed level change may cause vegetation to disappear (Willemsen et al., 2018). Bendoni et al. (2019) showed in a modelling study that vegetated saltmarshes can sustain a steeper cliff than bare saltmarshes. The effect of plant roots on stabilization may also be stronger when the mud content of the cliff edge is lower (Bendoni et al., 2019). Allen (1989) showed that a dense root mat at the surface of some sandy marshes may result in undercutting and mass failure. At our study site, a strip with die-off of aboveground vegetation was observed. Our marsh edge profiles typically did not show signs of undercutting. Instead, in 2018, a terraced, ramped marsh edge structure was formed where sediment provided resistance against erosion (cf. Fig. 4). The TLS maps (Electronic Supplementary Materials 4–6) further indicate that dents in the marsh edge may be the preferential location for further erosion (e.g., between 1 Sep 2016 and 20 Oct 2016, just west of the centre plot), which may have contributed to the spatial differences in the lateral erosion rate.

The SED sensors have provided a novel, high resolution perspective on saltmarsh erosion that would not have been possible by other methods. The local measurements clearly indicate an erosional trend with distinct periods with stronger and weaker erosion rates. Mel et al. (2022) demonstrated that the slope of the regression between the lateral erosion rate and wave power varied with elevation position at the cliff edge. Our results show that the cliff edge retreats and changes shape, and this might also change the local lateral erosion rate. Moreover, morphological changes may lead to changes in local hydrodynamics, and such a feedback mechanism may also preclude a simple linear relationship between wave energy and inundation duration, and lateral saltmarsh erosion on longer time-scales. Application of the SED sensors in other, contrasting sites is recommended to further elucidate the role of tides and waves in saltmarsh erosion under a range of external and internal conditions, and to further clarify the relationships between saltmarsh erosion and their position in the tidal frame. Technical improvements can be made by avoiding re-set/re-installment of the SED sensors to warrant un-interrupted time-series. In addition, multiple SED sensors at each site are recommended to improve the assessment. For TLS, care should be taken in areas with sparse data. Advanced handling of point cloud data may improve the representation of the marsh edge, particularly in case of sparse data or cliff undercutting. Consistent time-series would allow a direct intercomparison between TLS and SED sensors. The TLS point cloud data provide the spatial context for the SED data; they provide essential information of the cliff edge and mudflat geometry and allow to identify the location and volume of erosion/sedimentation of the unvegetated mudflat-saltmarsh transition over longer (ca monthly) time-scales. The process knowledge from these complementary data sets can then be used for upscaling results using satellite data (e.g., Laengner et al., 2019).

6. Conclusions

In this study, we monitored the saltmarsh-mudflat continuum for 2.5 years, using a Terrestrial Laser Scanner to quantify topographical changes at the saltmarsh-mudflat edge, SED sensors to quantify local lateral cliff retreat, and a pressure transducer to register wave and water level characteristics, as well as additional information on wind speed. We found that lateral cliff erosion was mostly gradual rather than episodic, but local lateral erosion rates varied in space, and in time, with occasional mass failure. Lateral erosion continued in the absence of storms, and common weather conditions were more important for the long-term erosion of the saltmarsh cliff than incidental wind or high wave energy events. The high spatial resolution and wider coverage of the TLS combined with the high temporal resolution of the SED sensors at point locations allow monitoring saltmarsh erosion at high spatio-temporal resolution.

Declaration of competing interest

The authors declare that they have no known competing financial interests or personal relationships that could have appeared to influence the work reported in this paper.

Data availability

Data collected and analysed for this paper are stored at the 4TU. Research repository. Daily and hourly wind data are available from the Royal Netherlands Meteorological Institute KNMI (https://www.knmi.nl/nederland-nu/klimatologie/daggegevens, station 315 Hansweert), 10 min wind data for Hansweert are available from Rijkswaterstaat (https://waterberichtgeving.rws.nl/water-en-weer/dataleveringen/ophalen-opgetreden-data).

Acknowledgements

This study was partially performed as contribution to the EU FAST FP7 project FAST (Foreshore Assessment using Space Technology, grant agreement 607131). We thank Lennart van IJzerloo (NIOZ) and Bas Oteman (NIOZ) for their help in the field, and Greg Fivash (NIOZ) for help with processing of the wave data. Sediment grain-size samples were analysed in the analytical laboratory of NIOZ.

Appendix A. Supplementary data

Supplementary data to this article can be found online at https://doi.org/10.1016/j.geomorph.2023.108590.

References

Adriaens, R., Zeelmaekers, E., Fettweis, M., Vanlierde, E., Vanlede, J., Stassen, P., Elsen, J., Środoń, J., Vandenberghe, N., 2018. Quantitative clay mineralogy as provenance indicator for recent muds in the southern North Sea. Mar. Geol. 398, 48–58. https://doi.org/10.1016/j.margeo.2017.12.011.

Allen, J.R.L., 1989. Evolution of salt-marsh cliffs in muddy and sandy systems: a qualitative comparison of British West-Coast estuaries. Earth Surf. Process. Landf. 14, 85–92. https://doi.org/10.1002/esp.3290140108.

Beckers, F., Inskeep, C., Haun, S., Schmid, G., Wieprecht, S., Noack, M., 2020. High spatio-temporal resolution measurements of cohesive sediment erosion. Earth Surf. Process. Landf. 45, 2432–2449. https://doi.org/10.1002/esp.4889.

Bendoni, M., Francalanci, S., Cappietti, L., Solari, L., 2014. On salt marshes retreat: experiments and modeling toppling failures induced by wind waves. J. Geophys. Res. Earth Surf. 119, 603–620. https://doi.org/10.1002/2013JF002967.

Bendoni, M., Mel, R., Solari, L., Lanzoni, S., Francalanci, S., Oumeraci, H., 2016. Insights into lateral marsh retreat mechanism through localized field measurements. Water Resour.Res. 52, 1446–1464. https://doi.org/10.1002/2015WR017966.

Bendoni, M., Georgiou, I.Y., Roelvink, D., Oumeraci, H., 2019. Numerical modelling of the erosion of marsh boundaries due to wave impact. Coast. Eng. 152, 103514 https://doi.org/10.1016/j.coastaleng.2019.103514.

Best, Ü.S.N., Van der Wegen, M., Dijkstra, J., Willemsen, P.W.J.M., Borsje, B.W., Roelvink, D.J.A., 2018. Do salt marshes survive sea level rise? Modelling wave action, morphodynamics and vegetation dynamics. Environ. Model Softw. 109, 152–166.

Bouma, T.J., van Belzen, J., Balke, T., Zhu, Z., Airoldi, L., Blight, A.J., Davies, A.J., Galván, C., Hawkins, S.J., Hoggart, S.P.G., Lara, J.L., Losada, I.J., Maza, M., Ondiviela, B., Skov, M.W., Strain, E.M., Thompson, R.C., Yang, S.L., Zanuttigh, B., Zhang, L., Herman, P.M.J., 2014. Identifying knowledge gaps hampering application of intertidal habitats in coastal protection: opportunities & steps to take. Coast. Eng. 87, 147–157.

Bouma, T.J., van Belzen, J., Balke, T., van Dalen, J., Klaassen, P., Hartog, A.M., Callaghan, D.P., Hu, Z., Stive, M.J.F., Temmerman, S., Herman, P.M.J., 2016. Short-term mudflat dynamics drive long-term cyclic salt marsh dynamics. Limnol. Oceanogr. 61, 2261–2275.

Cai, H., Savenije, H.G., Toffolon, M., 2013. The effect of river discharge on tidal dynamics in three alluvial estuaries: the Scheldt, Modaomen and Yangtze cases. In: Deltas: Landforms, Ecosystems and Human Activities. Proceedings of HP1, IAHS-IAPSO-IASPEI Assembly, Gothenburg, Sweden, July 2013, 358. IAHS Publ.

Callaghan, D.P., Bouma, T.J., Klaassen, P., van der Wal, D., Stive, M.J.F., Herman, P.M.J, 2010. Hydrodynamic forcing on salt-marsh development: Distinguishing the relative importance of waves and tidal flows. Estuar. Coast. Shelf Sci. 89, 73–88. https://doi.org/10.1016/j.ecss.2010.05.013.

Cao, H., Zhu, Z., Balke, T., Zhang, L., Bouma, T.J., 2018. Effects of sediment disturbance regimes on Spartina seedling establishment: implications for salt marsh creation and restoration. Limnol. Oceanogr. 63, 647–659.

Cooper, N.J., 2005. Wave dissipation across intertidal surfaces in the Wash tidal inlet, eastern England. J. Coast. Res. 21, 28–48.

Costanza, R., d'Arge, R., de Groot, R., Farber, S., Grasso, M., Hannon, B., Limburg, K., Naeem, S., O'Neill, R.V., Paruelo, J., Raskin, R.G., Sutton, P., van den Belt, M., 1997. The value of the world's ecosystem services and natural capital. Nature 387 (6630), 253–260.

Cracknell, A.P., 1999. Remote sensing techniques in estuaries and coastal zone: an update. Int. J. Remote Sens. 20, 485–496.

De Battisti, D., Fowler, M.S., Jenkins, S.R., Skov, M.W., Rossi, M., Bouma, T.J., Neyland, P.J., Griffin, J.N., 2019. Intraspecific root trait variability along environmental gradients affects salt marsh resistance to lateral erosion. Front. Ecol. Evol. 7, 150. https://doi.org/10.3389/fevo.2019.00150.

De Vet, P.L.M., Van Prooijen, B.C., Colosimo, I., Ysebaert, T., Herman, P.M.J., Wang, Z. B., 2020. Sediment disposals in estuarine channels alter the eco-morphology of intertidal flats. J.Geophys.Res.: Earth Surf. 125, e2019JF005432 https://doi.org/10.1029/2019JF005432.

Dennis, B., Civille, J.C., Strong, D.R., 2011. Lateral spread of invasive Spartina alterniflora in uncrowded environments. Biol. Invasions 13, 401–411.

Eleveld, M.A., van der Wal, D., van Kessel, T., 2014. Estuarine suspended particulate matter concentrations from sun-synchronous satellite remote sensing: tidal and meteorological effects and biases. Remote Sens. Environ. 143, 204–215.

Evans, B.R., Moeller, I., Spencer, T., 2019. Dynamics of salt marsh margins are related to their three-dimensional functional form. Earth Surf. Process. Landf. 44, 2826–2827.

Fagherazzi, S., Kirwan, M.L., Mudd, S.M., Guntenspergen, G.R., Temmerman, S., D'Alpaos, A., van de Koppel, J., Rybczyk, J.M., Reyes, E., Craft, C., Clough, J., 2012. Numerical models of salt marsh evolution: ecological and climatic factors. Rev. Geophys. 50, 1. https://doi.org/10.1029/2011RG000359.

Fagherazzi, S., Mariotti, G., Wiberg, P.L., McGlathery, K.J., 2013. Marsh collapse does not require sea level rise. Oceanography 26, 70–77. https://doi.org/10.5670/oceanog.2013.47.

Feagin, R.A., Lozada-Bernard, S.M., Ravens, T.M., Möller, I., Yeager, K.M., Baird, A.H., 2009. Does vegetation prevent wave erosion of salt marsh edges? Proc. Natl. Acad. Sci. 106, 10109–10113. https://doi.org/10.1073/pnas.0901297106.

Feist, B.E., Simenstad, C.A., 2000. Expansion rates and recruitment frequency of exotic smooth cordgrass, Spartina alterniflora (Loisel), colonizing unvegetated littoral flats in Willapa Bay, Washington. Estuaries 23, 287-274.

Francalanci, S., Bendoni, M., Rinaldi, M., Solari, L., 2013. Ecomorphodynamic evolution of salt marshes: experimental observations of bank retreat processes. Geomorphology 195, 53–65. https://doi.org/10.1016/j.geomorph.2013.04.026.

Gabet, E.J., 1998. Lateral migration and bank erosion in a saltmarsh tidal channel in San Francisco Bay, California. Estuaries 21, 745–753.

Guillou, N., 2020. Estimating wave energy flux from significant wave height and peak period. Renew. Energy 155, 1383e13931385.

Hammond, M.E.R., Malvarez, G.C., Cooper, A., 2002. The distribution of Spartina anglica on estuarine mudflats in relation to wave-related hydrodynamic parameters. J. Coast. Res. SI 36, 352–355.

Hu, Z., Lenting, W., van der Wal, D., Bouma, T.J., 2015a. Continuous monitoring bed-level dynamics on an intertidal flat: introducing novel, stand-alone high-resolution SED-sensors. Geomorphology 245, 223–230.

Hu, Z., van Belzen, J., van der Wal, D., Balke, T., Wang, Z.B., Stive, M., Bouma, T.J., 2015b. Windows of opportunity for saltmarsh vegetation establishment on bare tidal flats: the importance of temporal and spatial variability in hydrodynamic forcing. J. Geophys. Res. Biogeosci. 120, 1450–1469.

Hu, Z., Yao, P., van der Wal, D., Bouma, T.J., 2017. Patterns and drivers of daily bed-level dynamics on two tidal flats with contrasting wave exposure. NPG Sci.Rep. 7 (1), 7088. https://doi.org/10.1038/s41598-017-07515-y.

Hu, Z., van der Wal, D., Cai, H., van Belzen, J., Bouma, T.J., 2018. Dynamic equilibrium behaviour observed on two contrasting tidal flats from daily monitoring of bed-level changes. Geomorphology 311, 114–126.

Hu, Z., Willemsen, P.W.J.M., Borsje, B.W., Wang, C., Wang, H., van der Wal, D., Zhu, Z., Oteman, B., Vuik, V., Evans, B., Möller, I., Belliard, J.-P., Van Braeckel, A., Temmerman, S., Bouma, T.J., 2021. Synchronized high-resolution bed-level change and biophysical data from 10 marsh–mudflat sites in northwestern Europe. Earth Syst.Sci.Data 13 (2), 405–416. https://doi.org/10.5194/essd-13-405-2021.

Huff, T.P., Feagin, R.A., Delgado, A., 2019. Understanding lateral marsh edge erosion with terrestrial laser scanning (TLS). Remote Sens. 11 (19), 2208. https://doi.org/10.3390/rs11192208.

James, M.R., Quinton, J.N., 2014. Ultra-rapid topographic surveying for complex environments: the hand-held mobile laser scanner (HMLS). Earth Surf. Process. Landf. 39, 138–142. https://doi.org/10.1002/esp.3489.

Karimpour, A., Chen, Q., Twilley, R.R., 2016. A field study of how wind waves and currents may contribute to the deterioration of saltmarsh fringe. Estuar. Coasts 29, 935–950. https://doi.org/10.1007/s12237-015-0047-z.

Kirwan, M.L., Megonigal, J.P., 2013. Tidal wetland stability in the face of human impacts and sea-level rise. Nature 504, 53–60.

Knutson, P.L., Brochu, R.A., Seelig, W.N., Inskeep, M., 1982. Wave damping in Spartina alterniflora marshes. Wetlands 2, 87–104.

Ladd, C.J.T., Duggan-Edwards, M.F., Bouma, T.J., Pagès, J.F., Skov, M.W., 2019. Sediment supply explains long-term and large-scale patterns in salt marsh lateral expansion and erosion. Geophys. Res. Lett. 46, 11178–11187. https://doi.org/10.1029/2019GL083315.

Laengner, M.L., Siteur, K., van der Wal, D., 2019. Trends in the seaward extent of saltmarshes across Europe from long-term satellite data. Remote Sens. 11, 1653. https://doi.org/10.3390/rs11141653.

Lawler, D.M., 1991. A new technique for the automatic monitoring of erosion and deposition rates. Water Resour. Res. 27, 2125–2128.

Lawler, D.M., 1992. Design and installation of a novel automatic erosion monitoring system. Earth Surf. Process. Landf. 17, 455–463.

Lawler, D.M., West, J.R., Couperthwaite, J.S., Mitchell, S.B., 2001. Application of a novel automatic erosion and deposition monitoring system at a channel bank site on the tidal River Trent, UK. Estuar. Coast. Shelf Sci. 53, 237–247.

Lawler, D.M., Couperthwaite, J., Bull, L.J., Harris, N.M., 1997. Bank erosion events and processes in the Upper Severn basin. Hydrol. Earth Syst. Sci. 1, 523–534. https://doi.org/10.5194/hess-1-523-1997.

Leonardi, N., Ganju, N.K., Fagherazzi, S., 2016a. A linear relationship between wave power and erosion determines salt-marsh resilience to violent storms and hurricanes. Proc. Natl. Acad. Sci. 113, 64–68. https://doi.org/10.1073/pnas.1510095112.

Leonardi, N., Defne, Z., Ganju, N.K., Fagherazzi, S., 2016b. Salt marsh erosion rates and boundary features in a shallow bay. J. Geophys. Res. Earth Surf. 121, 1861–1875. https://doi.org/10.1002/2016JF003975.

Leonardi, N., Camacina, I., Donatelli, C., Ganju, N.K., Plater, A.J., Schuerch, M., Temmerman, S., 2018. Dynamic interactions between coastal storms and salt marshes: a review. Geomorphology 301, 92–107. https://doi.org/10.1016/j.geomorph.2017.11.001.

Lo, V.B., Bouma, T.J., van Belzen, J., Van Colen, C., Airoldi, L., 2017. Interactive effects of vegetation and sediment properties on erosion of salt marshes in the Northern Adriatic Sea. Mar. Environ. Res. 131, 32–42.

Ma, Z., Ysebaert, T., van der Wal, D., Herman, P.M.J., 2018. Conditional effects of tides and waves on short-term marsh sedimentation dynamics. Earth Surf. Process. Landforms 43, 2243–2255. https://doi.org/10.1002/esp.4357.

Marani, M., D'Alpaos, A., Lanzoni, S., Santalucia, M., 2011. Understanding and predicting wave erosion of marsh edges. Geophys. Res. Lett. 38, L21401. https://doi.org/10.1029/2011GL048995.

Marin-Diaz, M., Govers, L.L., van der Wal, D., Olff, H., Bouma, T.J., 2021. How grazing management can maximize erosion resistance of saltmarshes. J. Appl. Ecol. 58, 1533–1544. https://doi.org/10.1111/1365-2664.13888.

Mariotti, G., Fagherazzi, S., 2013. Critical width of tidal flats triggers marsh collapse in the absence of sea-level rise. Proc. Natl. Acad. Sci. 110, 5352–5356.

Mariotti, G., Carr, J., 2014. Dual role of salt marsh retreat: long-term loss and short-term resilience. Water Resour. Res. 50, 1944–7973.
McKee, K., Patrick, W.H., 1988. The relationship of smooth cordgrass (Spartina alterniflora) to tidal datums: a review. Estuaries 11, 143–151.
McLoughlin, S.M., Wiberg, P.L., Safak, I., McGlathery, K.J., 2015. Rates and forcing of marsh edge erosion in a shallow coastal bay. Estuar. Coasts 38, 620–638. https://doi.org/10.1007/s12237-014-9841-2.
Mel, R.A., Bendoni, M., Steffinlongo, D., 2022. Salt-marsh retreat on different time scales: issues and prospects from a 5-year monitoring campaign in the Venice Lagoon. Earth Surf. Process. Landf. 47, 1989–2005.
Millero, F.J., Poisson, A., 1981. International one-atmosphere equation of state of seawater. <sb:contribution><sb:title>Deep Sea Res. Part A.</sb:title></sb:contribution><sb:host><sb:issue><sb:series><sb:title><sb:maintitle check="true">Oceanogr. Res. Pap.</sb:maintitle></sb:title></sb:series></sb:issue></sb:host> 28, 625–629.
Möller, I., Kudella, M., Rupprecht, F., Spencer, T., Paul, M., van Wesenbeeck, B.K., Wolters, G., Jensen, K., Bouma, T.J., Miranda-Lange, M., Schimmels, S., 2014. Wave attenuation over coastal salt marshes under storm surge conditions. Nat. Geosci. 7, 727–731.
Nieuwhof, S., Herman, P.M.J., Dankers, N., Troost, K., van der Wal, D., 2015. Remote sensing of epibenthic shellfish using synthetic aperture radar satellite imagery. Remote Sens. 7, 3710–3734. https://doi.org/10.3390/rs70403710.
Pringle, A.W., 1995. Erosion of a cyclic saltmarsh in Morecambe Bay, North-West England. Earth Surf. Process. Landf. 20, 387–405. https://doi.org/10.1002/esp.3290200502.
Saye, S.E., van der Wal, D., Pye, K., Blott, S.J., 2005. Beach dune morphological relationships and erosion/accretion: an investigation at five sites in England and Wales using LIDAR data. Geomorphology 72, 128–155.
Schuerch, M., Spencer, T., Evans, B., 2019. Coupling between tidal mudflats and salt marshes affects marsh morphology. Mar. Geol. 412, 95–106.
Schwimmer, R.A., 2001. Rates and processes of marsh shoreline erosion in Rehoboth Bay, Delaware, U.S.A. J. Coast.Res. 17, 672–683. https://doi.org/10.2307/4300218.
Shilpakar, P., Oldow, J.S., Walker, J.D., Whipple, K.X., 2016. Assessment of the uncertainty budget and image resolution of terrestrial laser scans of geomorphic surfaces. Geosphere 12, GES01113.1. https://doi.org/10.1130/GES01113.1.
Siemes, R.W.A., Borsje, B.W., Daggenvoorde, R.J., Hulscher, S.J.M.H., 2020. Artificial structures steer morphological development of salt marshes: a model study. J. Mar. Sci. Eng. 8, 326. https://doi.org/10.3390/jmse8050326.
Singh Chauhan, P.P., 2009. Autocyclic erosion in tidal marshes. Geomorphology 110, 45–57. https://doi.org/10.1016/j.geomorph.2013.11.010.
Smith, G.L., Zarillo, G.A., 1990. Calculating long-term shoreline recession rates using aerial photographic and beach profiling techniques. J. Coast. Res. 6, 111–120.
Stumpf, R.P., 1983. The process of sedimentation on the surface of a saltmarsh. Estuar. Coast. Shelf Sci. 17, 495–508.
Tommasini, L., Carniello, L., Massimiliano, G., Roner, M., D'Alpaos, A., 2019. Changes in the wind-wave field and related salt-marsh lateral erosion: inferences from the evolution of the Venice Lagoon in the last four centuries. Earth Surf. Process. Landf. 44, 1633–1646.
Van de Koppel, J., van der Wal, D., Bakker, J.P., Herman, P.M.J., 2005. Self-organisation and vegetation collapse in salt marsh ecosystems. Am. Nat. 165, E1–E12.
van der Wal, D., Pye, K., Neal, A., 2002. Long-term morphological change in the Ribble Estuary, northwest England. Mar. Geol. 189, 249–266. https://doi.org/10.1016/S0025-3227(02)00476-0.
van der Wal, D., Wielemaker-van den Dool, A., Herman, P.M.J., 2008. Spatial patterns, rates and mechanisms of saltmarsh cycles (Westerschelde, the Netherlands). Estuar. Coast.Shelf Sci. 76, 357–368.
van der Wal, D., Pye, K., 2004. Patterns, rates and possible causes of saltmarsh erosion in the Greater Thames area (UK). Geomorphology 61, 373–391.
Wang, H., van der Wal, D., Li, X., van Belzen, J., Herman, P.M.J., Hu, Z., Ge, Z., Zhang, L., Bouma, T.J., 2017. Zooming in and out: scale dependence of extrinsic and intrinsic factors affecting salt marsh erosion. J.Geophys.Res.-Earth Surf. 122, 1455–1470. https://doi.org/10.1002/2016JF004193.
Willemsen, P.W.J.M., Borsje, B.W., Hulscher, S.J.M.H., van der Wal, D., Zhu, Z., Oteman, B., Evans, B., Möller, I., Bouma, T.J., 2018. Quantifying bed level change at the transition of tidal flat and salt marsh: can we understand the lateral location of the marsh edge? J. Geophys. Res. Earth Surf. 123, 2509–2524. https://doi.org/10.1029/2018JF004742.
Willemsen, P.W.J.M., Borsje, B.W., Vuik, V., Bouma, T.J., Hulscher, S.J.M.H., 2020. Field-based decadal wave attenuating capacity of combined tidal flats and salt marshes. Coast. Eng. 156, 103628 https://doi.org/10.1016/j.coastaleng.2019.103628.
Willemsen, P.W.J.M., Hortstman, E.M., Bouma, T.J., Baptist, M.J., van Puijenbroek, M.E.B., Borsje, B.W., 2022. Facilitating salt marsh restoration: the importance of event-based bed level dynamics and seasonal trends in bed level change. Front. Mar. Sci. 8, 793235 https://doi.org/10.3389/fmars.2021.793235.
Wolman, M.G., Miller, J.P., 1960. Magnitude and frequency of forces in geomorphic processes. J.Geol. 68, 54–74. https://doi.org/10.1086/626637.
Young, A.P., Ashford, S.A., 2008. Instability investigation of cantilevered seacliffs. Earth Surf. Process. Landf. 33, 1661–1677.
Young, A.P., Olson, M., Driscoll, N., Flick, R.E., Gutierrez, R., Guza, R.T., Johnstone, E., Kuester, F., 2010. Comparison of airborne and terrestrial lidar and estimates of seacliff erosion in Southern California. Photogramm. Eng. Remote Sens. 76, 421–427.
Zeileis, A., Kleiber, C., Krämer, W., Hornik, K., 2003. Testing and dating of structural changes in practice. Comput.Stat.Data Anal. 44, 109–123. https://doi.org/10.1016/S0167-9473(03)00030-6.
Zeileis, A., Leisch, F., Hornik, K., Kleiber, C., 2002. Strucchange: an R package for testing for structural change in linear regression models. J. Stat. Softw. 7, 1–38. https://doi.org/10.18637/jss.v007.i02.